



# Green Synthesis of Polylactic acid/Fe<sub>3</sub>O<sub>4</sub>@β-Cyclodextrin Nanofibrous Nanocomposite Loaded with *Ferulago Angulata* Extract as a Novel Nano-biosorbent: Evaluation of Diazinon Removal and Antibacterial Activity

Roya Behrooz, Dadkhoda Ghazanfari, Nahid Rastakhiz\*, Enayatollah Sheikhhosseini, Sayed Ali Ahmadi

Department of Chemistry, Kerman branch, Islamic Azad University, Kerman, Iran

\*Corresponding author: Nahid Rastakhiz, Department of Chemistry, Kerman Branch, Islamic Azad University, Kerman, Iran; Tel/Fax: +98-3431321338, E-mail: [n.rastakhiz@iauk.ac.ir](mailto:n.rastakhiz@iauk.ac.ir)

Received: 2023/08/19 ; Accepted: 2023/08/19

**Background:** Organophosphate pesticides are one of the most extensively applied insecticides in agriculture. These insecticides persist in the environs and thereby cause severe pollution problems. Iron oxide polymer nanocomposites are wastewater remediation agents synthesized by various methods. When compared to chemical processes, green synthesis using plant extract is thought to be more cost- and environmentally-friendly.

**Objectives:** This study aimed to evaluate the green synthesis of Fe<sub>3</sub>O<sub>4</sub>@β-Cyclodextrin (Fe<sub>3</sub>O<sub>4</sub>@β-CD) nanoparticles using *Ferulago angulata* (*F. angulata*) methanol extract. These nanoparticles are loaded on polylactic acid (PLA) nanofibrous nanocomposite along with *Ferulago angulata* extract (2, 4, and, 6wt %) to produce PLA/Fe<sub>3</sub>O<sub>4</sub>@β-CD/*F. angulata* extract nanofibrous nanocomposite as a new nano biosorbent. Furthermore, the antibacterial properties of this compound and its activity in diazinon removal have been evaluated.

**Materials and Methods:** Fe<sub>3</sub>O<sub>4</sub>@β-CD nanoparticles synthesis was performed via co-precipitation method using FeCl<sub>3</sub>·6H<sub>2</sub>O and FeCl<sub>2</sub>·4H<sub>2</sub>O and β-cyclodextrin, and *Ferulago angulata* extract. Then polylactic acid/ Fe<sub>3</sub>O<sub>4</sub>@β-CD / *F. angulata*.extract nanofibrous nanocomposite was prepared by the electrospinning method. Energy-dispersive X-ray spectroscopy (EDS), X-ray diffraction analysis (XRD), vibrating sample magnetometer (VSM), and Fourier transform infrared spectroscopy (FTIR) were used to analyze the structure of the nanocomposite. The antibacterial activity of this nanocomposite against several fish and human bacterial pathogens, as well as its effectiveness in diazinon elimination, have been evaluated in the sections that follow.

**Results:** The nanocomposite structure demonstrated that Fe<sub>3</sub>O<sub>4</sub> nanoparticles were produced and put into the polylactic acid matrix with an average particle size of 40 nm. Furthermore, the results showed that this nanocomposite exhibited removal efficiency of diazinon over 80% after 120 minutes under pH=7 and 2.5 gr.L<sup>-1</sup> nanocomposite concentration. Also, this structure showed above 70% antibacterial ability against *Bacillus cereus*, *Staphylococcus epidermidis* and 60% antibacterial ability against *Streptococcus iniae* and *Yersinia ruckeri*.

**Conclusion:** Fe<sub>3</sub>O<sub>4</sub> nanocomposite synthesis may be accomplished in a delicate and efficient manner by using *Ferulago angulata* to produce Fe<sub>3</sub>O<sub>4</sub>@β-CD nanoparticles. The stability of the nanoparticles was enhanced by combining *Ferulago angulata* extract with polylactic acid nanofibers to create an antibacterial homocomposition nanocomposite. This device may be used to remove and disinfect diazinon from aqueous media in an environmentally friendly manner.

**Keywords:** Diazinon, *Ferulago Angulata*, Iron oxide nanoparticles, Nanocomposite, Polylactic acid.

## 1. Background

Global pollution, especially water pollution and waste management, is recognized as an international public health issue that should be studied from multiple perspectives, including social, economic, and environmental aspects (1, 2). Water pollution from unsustainable agricultural practices poses severe risks to human health and the global ecosystem. Some organophosphorus pesticides, such as diazinon is widely used to control household insects and crops of fruits and vegetables. Diazinon is rated a moderate Class II chemical harmful to humans, aquatic animals, mammals, and other species by the World Health Organization (WHO) (3). It is relatively water-soluble and has a 40 mg. L<sup>-1</sup> solubility at 25 °C. For this reason, water systems contaminated with pesticides have been treated by various techniques such as filtration, membrane separation, and adsorption (4). Adsorption is considered as an efficient technique for pollution removal from wastewater effluents.

Recently, some low-cost and commercial adsorbents such as activated charcoal and bentonite have been used to eliminate pesticides with a maximum of 96% and 98% adsorption efficiency (5, 6).

Nevertheless, these adsorbents have limited porosity, surface area, and pores volume and rapidly lose their adsorption capacity. To overcome the conventional adsorbents' limitations, researchers introduced new generation adsorbents as nano adsorbents as novel efficient candidates for the water treatment system (7, 8). The nano-adsorbents can remove emerging pollutants even at low concentrations, i.e., µg.L<sup>-1</sup>, under different pH values and temperature conditions. One of the efficient nano-adsorbents is iron oxide nanoparticles used in biomedicine and water treatment (9, 10). These nanoparticles are suitable with the functionalization of chemical groups because they have a large specific surface area and a high capacity for pollutant adsorption. Also, biosorbents are other cost-effective adsorbents for removing toxic material from contaminated solutions. Biosorbents have other advantages, including simplicity, lack of chemical waste, easy desorption, and high biodegradation (11, 12).

Using nano biosorbents for environmental protection is a combinatorial approach that integrates nanotechnology with biomaterial to form nano bio-composites used as adsorbents to remove various contaminants from wastewater (13, 14).

Poly(lactic acid) (PLA) is one of the biodegradable aliphatic polyesters widely used in biocomposites preparation. It has unique properties such as excellent compatibility, absorbability, and degradation behavior in human bodies. Researchers have recently prepared some poly(lactic acid) composites containing nanoparticles in various fields (15). Another biomolecule that is used in the nano bio composite is cyclodextrin. Cyclodextrin is a water-soluble, non-toxic biomolecule that encapsulates bioactive molecules by forming nano-scale molecular inclusion complexes (16).

Additionally, other techniques have been created to create nanoparticles of varied sizes and forms (17, 18). The synthesis of nanoparticles by physical and chemical methods can cause significant environmental problems, technically and economically expensive. So, many reports present biological processes, microorganisms and enzymes, and plant extracts as possible eco-friendly alternatives (19-21).

Biosynthesis is a beneficial method because it reduces environmental impact compared with some physico-chemical synthesis methods and produces large quantities of uncontaminated nanoparticles with well-defined sizes and morphology. Recently, various plant extracts, such as *Garcinia mangostana* (22), *Kappaphycus alvarezii* (23), and *Moringa oleifera* (24), have acted as eco-friendly precursors to synthesize Fe<sub>3</sub>O<sub>4</sub>-NPs with the potential application.

*Ferulago angulata* Iran's central regions are home to the perennial plant boiss. The chemical makeup of the essential oil of *F. angulata* from various locations of Iran was disclosed by a review of studies (25-27).

## 2. Objectives

The major objective of the current work was to assess the new nano-biosorbent made from a green synthesized *Ferulago angulata*-loaded poly(lactic acid)/Fe<sub>3</sub>O<sub>4</sub>@β-Cyclodextrin nanofibrous nanocomposite. The following looks at this substance's antibacterial capabilities as well as its ability to remove diazinon

## 3. Materials and Methods

### 3.1. Materials

Purchased from Merck Company in Germany, the analytic-grade reagents FeCl<sub>3</sub>.6H<sub>2</sub>O, FeCl<sub>2</sub>.4H<sub>2</sub>O, and ammonia solution (25%) were used without additional purification. Sigma Aldrich Company in the US was

used to obtain polylactic acid with a molecular weight of 60000 Da, cyclodextrin, and dichloromethane. The Diazinon solution was bought (60%) from the Iranian Samsazan Company.

Some human pathogenic bacterial strains were the ones chosen for the antibacterial activity.

Including *Bacillus cereus* (PTCC 1665) and *Staphylococcus epidermidis* (PTCC 1435) as Gram-positive bacterial strains, *Salmonella enterica* (PTCC 1709), and *Escherichia coli* (PTCC 1399) as Gram-negative bacterial strains and some fish pathogenic bacterial strains such as *Vibrio fluvialis* (IBRC-M 10800), *Loctococcus garvieae* (IBRC-M 10900) *Yersinia ruckeri* (ATCC 29473) and *Streptococcus iniae* (ATCC 29178) were prepared from the Persian Type Culture Collection (PTCC) and Iranian Biological Resource Center (IBRC), Tehran, Iran.

### 3.2. Preparation of *Ferulago Angulata* Extract

In the beginning, new aerial portions of *Ferulago angulata* were procured from Kerman's Hezar mountain between April and June. The leaves were thoroughly cleaned to eliminate dust, let too dry at room temperature, and then pulverized into fine powders using a mortar. 50 g of finely chopped leaves were dissolved in 150 mL of 96% methanol and agitated magnetically for one hour at 60 °C to create *Ferulago angulata* extract. After being filtered using Whatman filter paper, the crude extract solution was dried in an oven for 24 hours at 45°C. For future use, the dried extract powder was kept at 4 °C.

### 3.3. Green Synthesis of $Fe_3O_4@β$ -CD NPs

For the synthesis of  $Fe_3O_4$ -NPs, firstly, a solution of 10 mL  $FeCl_3 \cdot 6H_2O$  (1M), 2 mL  $FeCl_2 \cdot 4H_2O$  (1M), and 0.3 gr  $β$ -cyclodextrin was added to the flask. The flask was then filled with 10 mL of *Ferulago angulata* extract, and it was rapidly agitated for 30 minutes at room temperature. The pH of the solution was then raised to 9 using an ammonia solution. Finally,  $β$ -cyclodextrin coated iron oxide nanoparticles appeared as black precipitation. Using a permanent magnet to separate the nanoparticles, they were then repeatedly rinsed in distilled water and ethanol before being dried overnight in an air oven at 45 °C. These nanoparticles were stored at 2-8 °C and protected from light until further characterization.

### 3.4. Preparation of PLA/ $Fe_3O_4@β$ -CD/ *F. Angulata* Extract Nano Fibrous Nanocomposite

Firstly, 2.0 g of PLA polymer was dissolved in 30 mL of  $CH_2Cl_2$  (10 wt. %). Then 0.2g of dried  $β$ -CD/ $Fe_3O_4$  NPs and *Ferulago angulata* extract (2, 4, and 6 %) were added to the PLA solution and sonicated for 15 min to form a uniform solution. A 5 mL plastic syringe fixed to a micro-injection pump in an electrospinning machine (NANOAZMA, model side by side, Iran) was filled with the combined solution. Voltage of 17 kV, flow rate of 0.5 mL.min<sup>-1</sup>, and tip-to-collector distance of 12 cm were the electrospinning parameters. The nanofibers were collected on aluminum foil after an hour, and any remaining solvent was subsequently evaporated over a 24-hour drying period at 40 °C.

### 3.5. Characterization

The synthesized  $Fe_3O_4@β$ -CD NPs and PLA/ $Fe_3O_4@β$ -CD nanofibrous nanocomposite were characterized using a variety of techniques, including scanning electron microscopy (SEM, model: Mira 3-TESCAN), X-ray spectroscopy (EDS, model SAMx), X-ray diffraction, and Fourier-transform infrared spectroscopy (FTIR). SEM was used to assess the size and surface morphology of  $Fe_3O_4@β$ -CD nanoparticles and nanofibers. Image J software (National Institutes of Health version 1.48v) was used to quantitatively assess the high-resolution SEM pictures of the samples. Crystallite sizes of  $Fe_3O_4@β$ -CD nanoparticles were recorded using a powder X-ray diffractometer (PW3064, Philips, Cu K<sub>α</sub> radiation ( $λ$  1.54 Å) with a scanning range ( $2θ$ ) from 4° ~ 90°.

The elemental analysis was assessed by EDS at an accelerating voltage of 100 kV. Shimadzu's IRTracer-100 spectrophotometer was used to perform FTIR at a wavenumber of 4000-400 cm<sup>-1</sup>.

The magnetic property of  $Fe_3O_4@β$ -CD NPs and PLA/ $Fe_3O_4@β$ -CD/*F. angulata* extract nanofibrous nanocomposite was studied by VSM technique using LKBFB device from "Magnetic Kavir Kashan" with a maximum magnetic field of 2.0 T at 298 K.

### 3.6. Diazinon Removal Experiment

By monitoring the rate of diazinon adsorption under various circumstances in accordance with the literature, the adsorption capability of the PLA/  $Fe_3O_4@β$ -CD/*F. angulata* extract nanofibrous nanocomposite was assessed (28).

First, 5 mg of diazinon was dissolved in 500 mL of distilled water to create the stock solution (10 mg. L<sup>-1</sup>). In a typical experiment, 500 mL of diazinon solution (10 mg. L<sup>-1</sup>) was added together with a specific amount of 1 g of the PLA/ Fe<sub>3</sub>O<sub>4</sub>@-CD/F. angulata extract nanofibrous nanocomposite as an adsorbent. Aqueous NaOH or HCl (0.1 mol.L<sup>-1</sup>) was used to bring the solution's original pH down to pH=7. For 30 minutes, the suspension was shaken and adjusted.

After decanting the combination, the residual diazinon concentrations were determined at 247 nm using a UV-Visible spectrophotometer (6305, Jenway, United Kingdom).

Some experiments were designed according to the different conditions to investigate the influential factors on nanocomposite efficiency as pH and initial diazinon concentration. The studies were conducted the same way with 1, 1.5, 2, 2.5, and 3 g.L<sup>-1</sup> at pH 3, 5, 7, 9, and 11. Nanofibrous nanocomposite of PLA/Fe<sub>3</sub>O<sub>4</sub>@-CD/F.

angulata extract, at diazinon doses of 10, 15, 20, 25, and 30 mg.15, 30, 45, 60, 75, 90, 105, and 120 minutes of contact time with L-1. Equation 1 was used to calculate the percentage of diazinon elimination:

Equation 1:

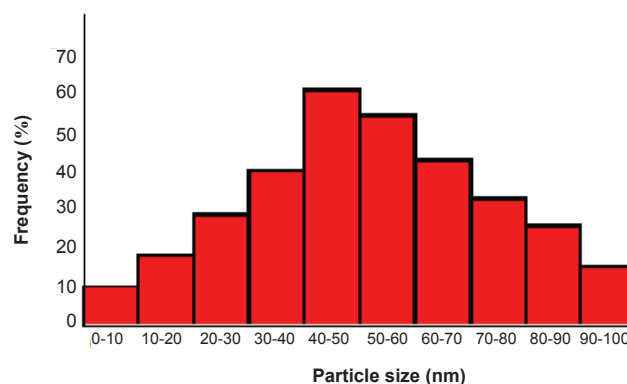
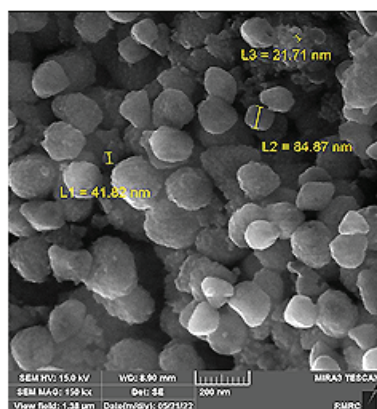
$$R=(C_0-C_t)/C_t \times 100$$

The viability of the nanocomposite for practical use was also tested through tests. Six successive tests were performed on a nanocomposite with a consistent composition for this purpose. The adsorbent was collected after each use, soaked in water for two hours, rinsed with methanol, dried for at least two hours at 100 °C, and then reused under the same diazinon removal conditions.

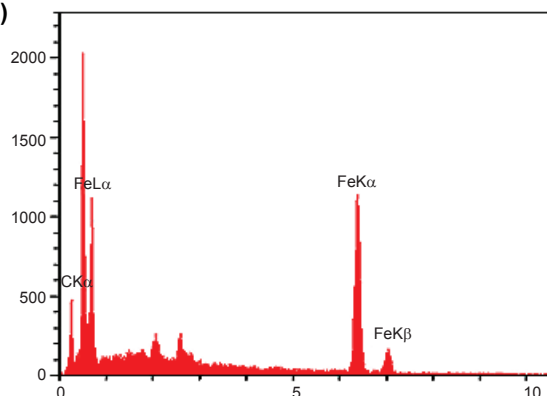
### 3.7. Antibacterial Activity

The colony count technique was used to examine the antibacterial activity of the polylactic acid/ Fe<sub>3</sub>O<sub>4</sub>@-Cyclodextrin/F. angulata extract nanofibrous nanocomposite against certain Gram-positive, Gram-

A)



B)



Elt	W%	A%
C	35.39	39.53
O	33.00	22.27
Fe	31.61	38.19

**Figure 1. Characterization of Fe<sub>3</sub>O<sub>4</sub>@β-CD nanoparticles. A) The SEM image and the size distribution histogram B) EDS analysis.**

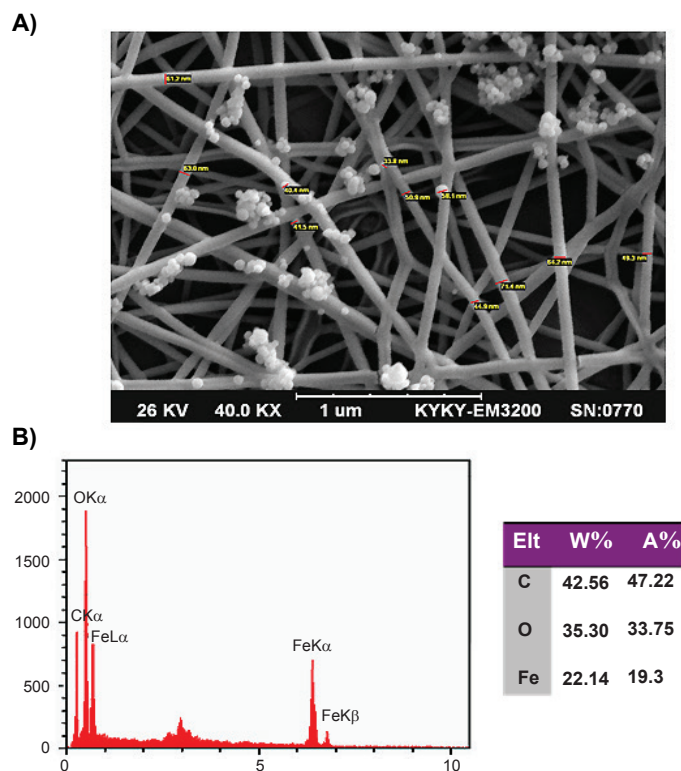


**Figure 2. Characterization of PLA/ Fe<sub>3</sub>O<sub>4</sub>@β-CD/ F. angulate.extract nanofibrous nanocomposite.**  
A) SEM images, B) EDS analysis.

negative, and fish pathogenic bacterial strains (29). The samples of the nanofibrous mat were first sterilized by being exposed to UV light for 15 minutes. Following that, 1 mL of bacterial suspensions containing  $1.5 \times 10^8$  CFU per mL were added to the nutritional broth. Following that, bacterial solution-filled circular discs made of nanofibrous mats ( $2.5 \times 2.5$  cm) were cultured at 37 °C for 72 hours. Equation 2 was used to compute the bacterial decrease at the end:

Equation 2:

$$\text{Bacterial reduction (\%)} = (B-A)/B \times 100$$

It is based on the quantity of colonies that developed in Petri plates before (B) and after (A), respectively, treatment with the sample.

## 4. Result

### 4.1. Characterization of Fe<sub>3</sub>O<sub>4</sub>@β-CD Nanoparticles

The SEM image and the size distribution histogram revealed green synthesized Fe<sub>3</sub>O<sub>4</sub>@β-CD nanoparticles were 40-80 nm with homogeneously spherical morphology. (Fig. 1A). The elemental analysis with EDS

showed three prominent peaks for carbon (35%), oxygen (33%), and iron (31%) that confirmed Fe<sub>3</sub>O<sub>4</sub>@β-CD nanoparticles synthesis. The minor peak shown in the EDS graph was due to trace impurities in the sample (Fig. 1B).

Figure S1 compares the XRD patterns of Fe<sub>3</sub>O<sub>4</sub>@-CD nanoparticles with those of Fe<sub>3</sub>O<sub>4</sub> nanoparticles and cyclodextrin. Fe<sub>3</sub>O<sub>4</sub> nanoparticles were responsible for the observed diffraction peaks at 2 values of 30.84, 35.51, 44.03, 53.17, 57.23, and 64.27, which correspond to lattice planes (220), (311), (400), (422), (511), and (440), respectively. Diffraction peaks at 2 values of 25.37 and 32.41, ascribed to cyclodextrin, were observed. These distinct peaks supported the hypothesized structure and indicated that the Fe<sub>3</sub>O<sub>4</sub> nanoparticle was stabilized in cyclodextrin.

### 4.2. Characterization of PLA/ Fe<sub>3</sub>O<sub>4</sub>@β-CD/ F. Angulate. Extract Nano Fibrous Nanocomposite

The SEM image of the nanocomposite is displayed in Figure 2A. With an average diameter of 65 nm and no beads, the nanocomposite contains homogeneous,

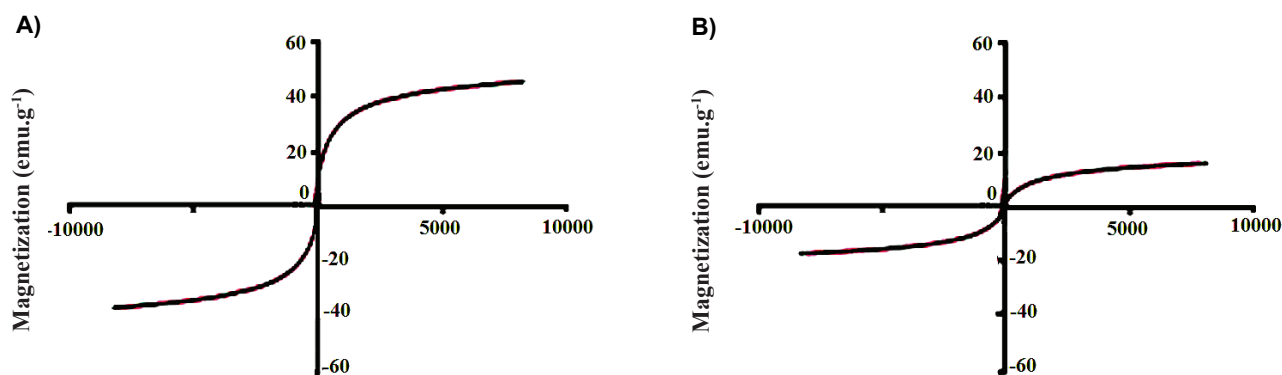


**Figure 3.** The magnetic hysteresis loop curves .A)  $\text{Fe}_3\text{O}_4@ \beta\text{-CD}$  nanoparticles and B) PLA/  $\text{Fe}_3\text{O}_4@ \beta\text{-CD}$ / *F. angulata*.extract nanofibrous nanocomposite.

smooth nanofibers. The nanofiber structure contains  $\text{Fe}_3\text{O}_4$  nanoparticles that have an average particle size of 40 nm. Furthermore, the elemental analysis performed using the EDS method revealed three primary peaks for the elements C, O, and Fe, indicating that the PLA/  $\text{Fe}_3\text{O}_4@ \beta\text{-CD}$  nanofibrous nanocomposite was successfully synthesized. (Fig. 2B)

The (C-O), (C=O), (C=C), (C-H), and (OH) stretching bands are each represented by distinctive absorption bands at 1270, 1455, 1635, 2996, and 3501  $\text{cm}^{-1}$ , respectively, in the nanocomposite's FTIR spectrum analysis. Additionally, this structure's spectra displayed a large peak at roughly 495  $\text{cm}^{-1}$ , which corresponds to the chemical interaction between Fe and O in the nanocomposite. (Fig. S2)

The VSM curve of the nanocomposite is shown in **Figure 3**. Magnetic properties of PLA/ $\text{Fe}_3\text{O}_4@ \beta\text{-CD}$ / *F. angulata* extract nanofibrous nanocomposite was found to be 18.91  $\text{emu. g}^{-1}$ , while the  $\text{Fe}_3\text{O}_4@ \beta\text{-CD}$  NPs showed a higher magnetic value (42.31  $\text{emu. g}^{-1}$ ).

### 4.3. Adsorption Activity

#### 4.3.1. Effect of Adsorbent Dosage

By adjusting the adsorbent doses from 1 to 3  $\text{g.L}^{-1}$  while maintaining the diazinon concentration (10  $\text{mg.L}^{-1}$ ) and pH 7 constants, the effects of adsorbent dosages on diazinon removal were examined. **Figure 4A** demonstrates how the diazinon removal capacity rose when the adsorbent dose was increased, reaching 85% at 3  $\text{g.L}^{-1}$ .

#### 4.3.2. Effect of Concentration of Diazinon

By adjusting the starting concentration of diazinon from 10 to 30 mg, the adsorption of diazinon by PLA/ $\text{Fe}_3\text{O}_4@ \beta\text{-CD}$ /*F. angulata* extract nanocomposite was examined.  $\text{L}^{-1}$  with a continuous dose of the nanocomposite (2.5  $\text{g. L}^{-1}$ ) and an initial pH of 7 (**Fig. 4B**). By raising the initial diazinon concentration from 10 to 30 mg, the outcomes were demonstrated.  $\text{L}^{-1}$ , the adsorption of diazinon dropped from 92 to roughly 56% after 120 minutes.

#### 4.3.3. Effect of Initial pH

In this work, the pH solution's impact on the adsorption of diazinon was investigated by altering it from 3 to 11 while maintaining a consistent dose of the nanocomposite (2.5  $\text{g.L}^{-1}$ ) and constant diazinon content (10  $\text{mg.L}^{-1}$ ). As shown in **Figure 4C**, the highest removal capacity appears at pH=7 (91%).

#### 4.3.4. Adsorbent Reusability

One benefit of the adsorption system to assess if the method is practicable for use is the reusability of the adsorbent. In this work, the reusability of the nanocomposite was examined after reusability tests were conducted six times. The outcomes are shown in **Figure S3**. It demonstrates unequivocally that even after three recycling cycles, the nanocomposite's ability to remove diazinon was unaffected. Although the removal percentage decreased after six times of recycling, adsorption capacity still possessed more than 80%. The result suggests that the adsorbent could be stable during the removal experiments and applied to environmental remediation for wastewater handling.

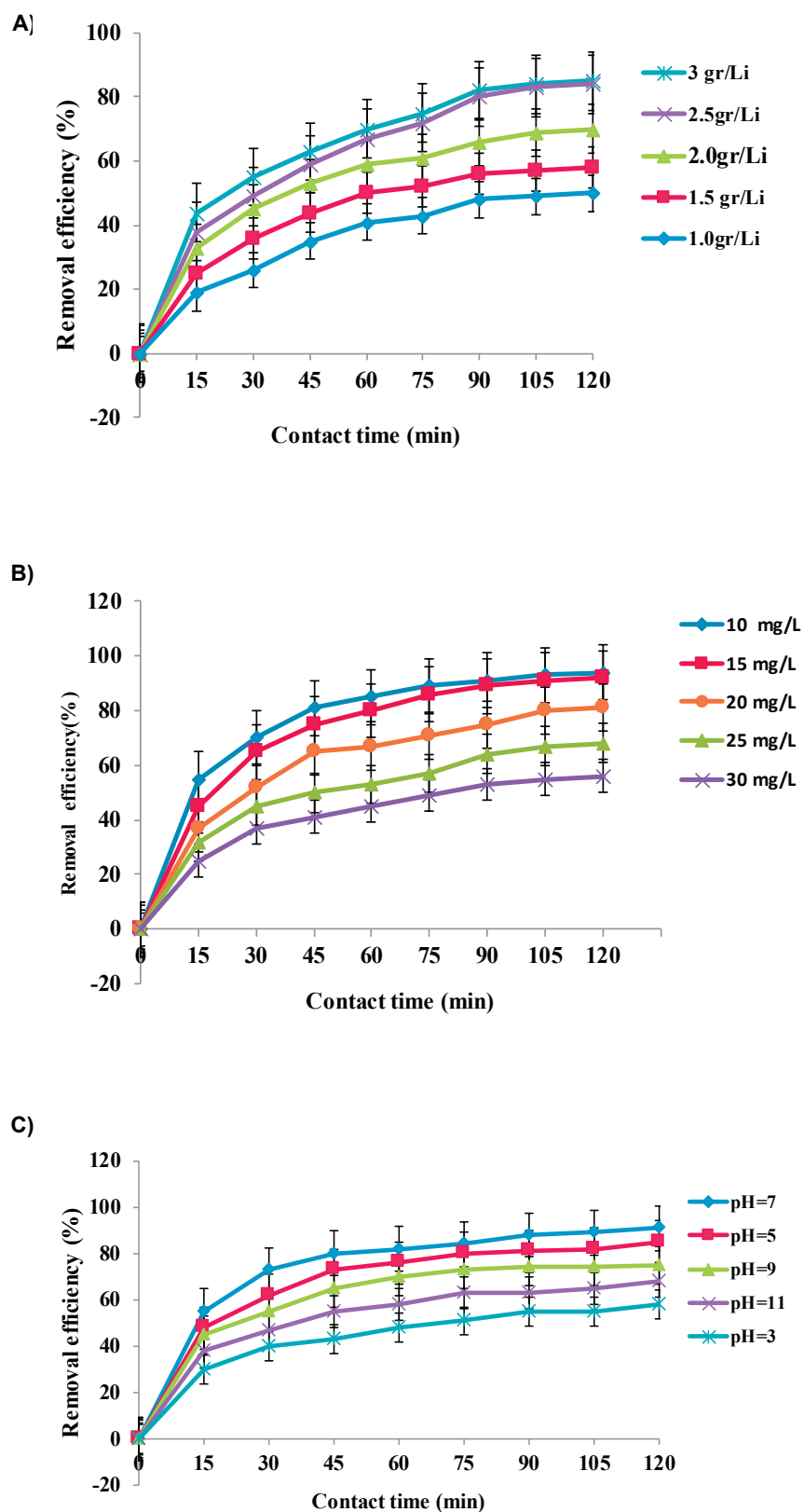
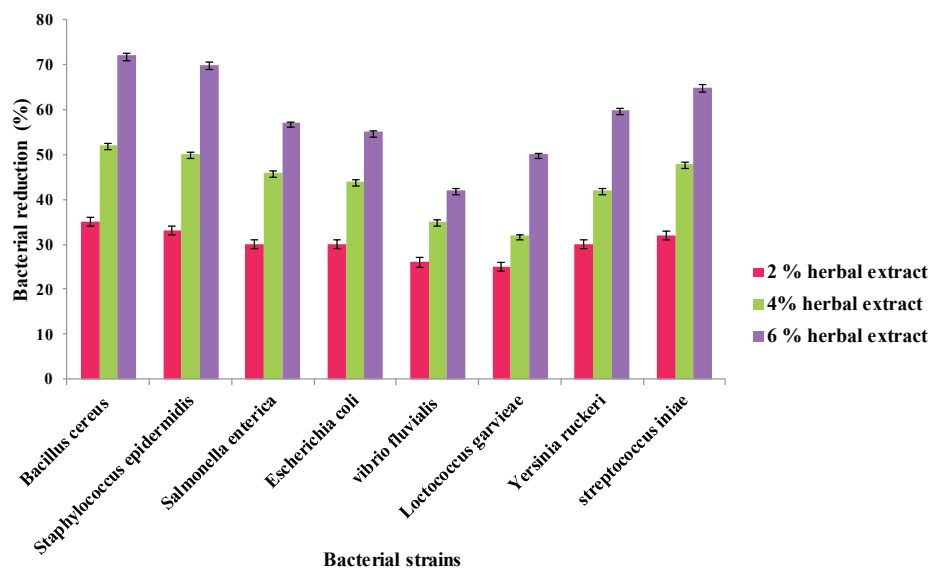


Figure 4. Impact of parameters on adsorption of diazinon onto PLA/Fe<sub>3</sub>O<sub>4</sub>@β-CD nanofibrous nanocomposite . A) Effect of adsorbent dosage and B) Effect of initial concentration of diazinon. C) Effect of initial pH on the adsorption of diazinon onto PLA/Fe<sub>3</sub>O<sub>4</sub>@β-CD nanofibrous nanocomposite .xlsx



**Figure 5. Antibacterial activity of PLA/ Fe<sub>3</sub>O<sub>4</sub>@β-CD/ F. angulata.extract nanofibrous nanocomposite against some fish and human bacterial pathogens.**

#### 4.3.5. Adsorption Kinetic

Based on the Langmuir-Hinshelwood method, estimated reaction rate constants for diazinon adsorption were derived.

$$\ln(C_0/C_t) = kt$$

The first-order rate constant is  $k$  (min<sup>-1</sup>), the diazinon concentration at response time ( $t$ ) is  $C_t$ , and  $C_0$  is the initial concentration of diazinon (Fig. S4). This nanocomposite was discovered to have a considerable diazinon reduction potential since the findings demonstrated that the adsorption rate increased in the time order. The results obtained from the adsorption isotherms and parameters for the diazinon adsorption by the nanocomposites are shown in Figure S5 and Table 1 respectively. In Langmuir isotherms  $C_e$  is the equilibrium concentration of diazinon in the solution and  $q_e$  denotes the amount of diazinon adsorbed at equilibrium. The plots of  $C_e/q_e$  versus  $C_e$  in Figure S5 indicate good linear correlations for adsorption.

#### 4.4. Antimicrobial Activity

Figure 5 depicts the results of the calculation used to determine the antibacterial activity of nanocomposites, which used a percentage decrease in the number of bacteria in the sample. Researchers looked at how different *F. angulata* extract concentrations (2, 4, and 6%) in nanocomposite affected bacterial infections in fish

and humans (gram-positive and gram-negative bacteria). The results showed nanofibrous nanocomposites loaded with *F. angulata* (6 wt. %) showed above 70% reductions in CFU.mL<sup>-1</sup> against *Bacillus cereus* and *Staphylococcus epidermidis*, and above 60% antibacterial ability against *Streptococcus iniae* and *Yersinia ruckeri*. *Bacillus cereus*, a human pathogenic bacterium, was extremely sensitive to the nanocomposites and had the most notable decrease in bacterial colonization, as seen by the antibacterial activity graph.

## 5. Discussion

The goal of this research was to create a green synthesis process for the Fe<sub>3</sub>O<sub>4</sub>@-CD nanoparticles needed to create a novel nanobioabsorbent composed of PLA/Fe<sub>3</sub>O<sub>4</sub>@-CD/*F. angulata* extract nanofibrous nanocomposite. Although, in recent years, many chemical methods have been developed to synthesize Fe<sub>3</sub>O<sub>4</sub> nanoparticles (30-32), chemistry-based Fe<sub>3</sub>O<sub>4</sub> nanoparticle synthesis has certain limitations, such as excessive waste products, high adsorbent cost, and the adsorbent's purification. Fe<sub>3</sub>O<sub>4</sub> nanoparticle green synthesis has therefore been suggested as an environmentally benign alternative to synthetic chemical processes. (33).

Further, in the chemical method, Iron oxide nanoparticles can be synthesized by coprecipitation of Fe<sup>2+</sup> and Fe<sup>3+</sup> by adding a base such as sodium hydroxide or ammonium

hydroxide. In green synthesis, these strong bases are replaced with plant extract and weak bases, and synthesis is performed in mild conditions. Furthermore, hydroxyl and carbonyl groups are the most important chemical components in the plant extract. Plant extract was able to perform as a stabilizing and reducing agent thanks to both functional groups.

In this work, we used the methanol extract of *Ferulago angulata*, a unique and natural plant of Iran, to create  $\text{Fe}_3\text{O}_4$  nanoparticles. Plant extract-based green synthesis of  $\text{Fe}_3\text{O}_4$  nanoparticles outperforms chemical approaches in terms of energy consumption, ease of use, low cost, and lack of use of significant quantities of harmful chemicals.

Studies on *Ferulago angulata* methanol extract revealed that the primary components were monoterpene chemicals such as g-terpinolene (11.97%),  $\alpha$ -pinene (10.00%), sabinene (6.89%), linalool (5.56%), and cis-ocimene (4.41%) (34). These organic compounds act as reducing agents in  $\text{Fe}_3\text{O}_4$  NPs synthesis.

The major components recovered from *Ferulago angulata* extract appear to be monoterpene chemicals, which are thought to be responsible for the formation of  $\text{Fe}_3\text{O}_4$  nanoparticles. It is thought that they could function as the surface molecules that are involved in the creation of nanoparticles, stabilizing and reducing nanoparticles. By the existence of functional terpenoids, such as C=C, C=O, and -C-O-C groups, reduction and stabilization are distinguished. Insufficient concentrations of terpenoids may also cause them to get adsorbed on the surfaces of metal nanoparticles, potentially through interactions with carbonyl groups or electrons in the absence of additional ligating solid agents.

One of the significant challenges in applying  $\text{Fe}_3\text{O}_4$  to aqueous media is nanoparticle stability and uniform dispersion. Homogeneous dispersion of  $\text{Fe}_3\text{O}_4$ -NPs in aqueous media is usually difficult due to the high surface energy and tendency to agglomerate. In this study,  $\beta$ -cyclodextrin is used as a coating agent to help offset this high surface energy and lead to nanoparticle stability.

Furthermore, when  $\text{Fe}_3\text{O}_4$ -NPs are coated with  $\beta$ -cyclodextrin, an interaction between the  $\text{Fe}_3\text{O}_4$ -NPs and O-H bond occurs, decreasing Fe-O bonding in nanoparticles and preventing its accumulation of nanoparticles.

$\text{Fe}_3\text{O}_4@ \beta$ -CD nanoparticles produced in this project by green strategy is a black powder with a high superparamagnetic property. By putting a magnetic bar

next to the flask, the magnetic response of  $\text{Fe}_3\text{O}_4$  was examined. Under the influence of an external magnetic field, the magnetite  $\text{Fe}_3\text{O}_4$  was easily isolated from the reaction medium due to the attraction of the black particles to the magnet.

$\text{Fe}_3\text{O}_4@ \beta$ -CD nanoparticles characterization was carried out using SEM, EDX, and XRD analysis.

The FESEM images, the size distribution histogram and EDX analysis confirming the  $\text{Fe}_3\text{O}_4@ \beta$ -CD synthesis.

**(Fig. 1)**

X-ray diffraction investigation validated the structure of  $\text{Fe}_3\text{O}_4$ -NPs nanoparticles (**Fig.S1**).

When the observed XRD pattern is compared to the standard ICDD card data 01-085-1436, all peaks match the standard ICDD, indicating that the  $\text{Fe}_3\text{O}_4$ -NPs are hexagonal and stable in the  $\beta$ -CD.(35)

Further, in this study, we successfully fabricated *Ferulago angulata* extract loaded PLA/ $\text{Fe}_3\text{O}_4@ \beta$ -CD nanofibrous nanocomposite and confirmed the possibility of the antibacterial nanofiber web as a new material.

PLA/ $\text{Fe}_3\text{O}_4@ \beta$ -CD/*F. angulata* extract nanofibrous nanocomposite is a gray coating insoluble in water. FESEM pictures of the nanocomposite's morphological structure indicated that the electro spun nanofibers' smooth, bead-free surface had  $\text{Fe}_3\text{O}_4$  nanoparticles that were uniformly disseminated throughout the nanofiber matrix.

FTIR spectroscopy of PLA/ $\text{Fe}_3\text{O}_4@ \beta$ -CD/*F. angulata* extract nanocomposite compared with FTIR spectrum of polylactic acid, cyclodextrin and  $\text{Fe}_3\text{O}_4$ , shows the functional groups of nanocomposite (**Fig. S2**). A large peak for the OH group, as determined by the cyclodextrin IR spectra, was seen in this spectrum at  $3501 \text{ cm}^{-1}$ . Additionally, the PLA/ $\text{Fe}_3\text{O}_4@ \beta$ -CD nanocomposite's FTIR spectra showed vibrations of the carbonyl group at  $1455$  and  $1759 \text{ cm}^{-1}$ . In addition, the IR spectra of  $\text{Fe}_3\text{O}_4$  revealed a large peak at  $495 \text{ cm}^{-1}$  showing the existence of the Fe-O group. Additionally, the peak of around  $1635 \text{ cm}^{-1}$  in the infrared spectrum of this nanocomposite can be linked to the stretching vibration bond of alkene groups attributable to monoterpene chemicals in *F. angulata* extract. These outcomes are comparable to those of previous papers (36).

The VSM curve of PLA/ $\text{Fe}_3\text{O}_4@ \beta$ -CD/*F. angulata* extract nanofibrous nanocomposite, and  $\text{Fe}_3\text{O}_4@ \beta$ -CD NPs is shown in **Figure 3**. As expected, the nanocomposite showed a lower magnetic value ( $18.91 \text{ emu. g}^{-1}$ ) compared to  $\text{Fe}_3\text{O}_4@ \beta$ -CD nanoparticles

(about 42.33 emu. g<sup>-1</sup>). This reduction is due to coating nanofibers layer on the surface of Fe<sub>3</sub>O<sub>4</sub>@β-CD NPs. Additionally, the results showed that PLA/Fe<sub>3</sub>O<sub>4</sub>@β-CD/ *F. angulata* extract nanofibrous nanocomposite is an effective adsorbent for the adsorption of diazinon. So, a variety of elements, including the amount of nanocomposite used, the initial concentration of diazinon, and the solution's pH, might influence the absorbance.

Increased doses of the PLA/Fe<sub>3</sub>O<sub>4</sub>@-CD/*F. angulata* extract nanofibrous nanocomposite enhance the surface's accessibility, the amount of diazinon that comes into contact with the adsorbent, and the effectiveness of the adsorption procedure. Above 2.5 g.L<sup>-1</sup>, there was no discernible change in clearance efficiency; hence, this was chosen as the ideal dosage.

In addition, the adsorption of diazinon dropped from 94% to 56% after 120 minutes when the starting concentration of diazinon was increased from 10 to 30 mg.L<sup>-1</sup>. This pattern was most likely explained by higher diazinon adsorption on the surface of the nanocomposite, which occupied all of the surface's active adsorption sites and lowered the adsorption rate with increasing diazinon concentrations. The findings matched those in the literature, which was reported (37).

As illustrated in **Figure 4C**, the nanocomposite's adsorption capability was investigated in relation to pH. It has been discovered that, when there is an adsorbent present, the adsorption capacity steadily rises with an increase in pH of 3–7. Additionally, the maximal adsorption capacity is reached at a pH of 7. Adsorption capability steadily declines at pH levels higher than 7. It might be as a result of the hydroxyl in cyclodextrin being affected by the hydrogen or hydroxide ion in the solution under acidic or alkaline circumstances, preventing diazinon from adhering to the surface.

The amount of the substance adsorbed onto the nanocomposite as an adsorbent and the concentration of the material adsorbed into the solution in equilibrium are related in a way expressed by adsorption isotherms. The experimental data were fitted using the most popular adsorption models, Langmuir and Freundlich. The Langmuir model, which has an adequate fit for the data of this study and a correlation coefficient equal to (R<sup>2</sup>) 0.9756, is determined by looking at the graph associated with each model and the value of the correlation coefficient between the model and the experimental data. The nanocomposite adsorbent is

chemically adsorbent and single-layer coated with diazinon, according to the fit of the Langmuir model to the experimental data collected in this work. In other words, the Langmuir model predicts that the adsorption of diazinon from the solution occurs as a result of the creation of a uniform monolayer of adsorbent at specified homogenous locations on the surface of nanocomposites, with no migration (38, 39).

The primary mechanism of diazinon adsorption by nanocomposites was proposed by Hydrogen bonding and π–π interaction. The creation of H-bonds and the absorption of diazinon by nanofiber adsorbents are caused by sulfur and oxygen atoms from the organophosphate backbone in diazinon.

Additionally, due to the aromatic structure of the diazinon molecule, it is thought that adsorption through electron interaction through “π–π” stacking between the adsorbent surface unsaturated bonds and the diazinon aromatic ring will play a substantial role in the absorption of diazinon in this situation.

Other nanocomposites such as magnetic tragacanth-montmorillonite nanocomposites (40), Fe<sub>3</sub>O<sub>4</sub>@SiO<sub>2</sub> magnetic nanocomposites (41) and magnetic bentonite nanocomposites (42) have been used in the diazinon adsorption. However, it seems that the sorption capacity of the developed nanocomposite is higher than other nanocomposites because of combination of nanofibers and magnetic nanoparticles. This nanocomposite also exhibits increased permeability as a result of the larger porosity and more tightly spaced pore sizes produced by the nanofibers.

Moreover the antibacterial activity of the synthesized nanocomposite is essential in water disinfection and agricultural utility. Infection, which happens when bacteria proliferate in water and may contain pathogens that can occasionally cause sickness and even death, is one of the biggest issues in water treatment.

Nanocomposite containing herbal extract is currently being investigated as an antibacterial agent against a wide range of pathogenic bacteria (43).

This investigation found that the antibacterial properties of the PLA/ Fe<sub>3</sub>O<sub>4</sub>@-CD/*F. angulata* extract nanofibrous nanocomposite were satisfactory against gram-positive and gram-negative bacteria as well as fish bacterial pathogens. Gram-positive bacteria like *Bacillus cereus* and *Staphylococcus epidermidis* were the most susceptible to this nanocomposite when compared to other types of bacteria, and they displayed the greatest

reduction in bacterial colonization.

These findings support Rania Dadi's findings that Gram-negative bacteria are more resistant to antibiotics than Gram-positive bacteria. (44), which might be ascribed to differences in the make-up of cell walls.

The cell wall of gram-positive bacteria is relatively thin, made up of a single layer, and allows for easy penetration of the antibacterial agent. In contrast, the cell wall of gram-negative bacteria is made up of multiple layers, acts as a strong protective barrier, and prevents antibacterial agent penetration.

The results indicated that the PLA/ Fe<sub>3</sub>O<sub>4</sub>@β-CD/ *F. angulata* extract nanofibrous nanocomposite demonstrated a significant antimicrobial effect in 6% concentrations of the extract. Herein, embedding the *Ferulago angulata* extract in nanofibers could increase penetration of extract and consequently enhance antibacterial activities.

## 6. Conclusion

Due to their high surface area-to-volume ratio and interconnected porous structure, nanofibrous nanocomposites are effective polymeric membranes for adsorption. In the current work, a new nanobiosorbent was created using a PLA/Fe<sub>3</sub>O<sub>4</sub>@-CD/*F. angulata* extract nanofibrous nanocomposite. Successful bead-free, smooth nanofibers with uniformly dispersed Fe<sub>3</sub>O<sub>4</sub>@-CD-NPs were visible in the morphology of the nanocomposite. Antibacterial studies of nanocomposite against some fish and human bacterial pathogens revealed reliable antibacterial properties. Further, the adsorption evaluation of the nanocomposites demonstrated effective absorbents with excellent stability for diazinon removal. In conclusion, this nanocomposite can be used as a helpful Nano bio sorbent and an effective antimicrobial agent in water treatment applications.

## References

- Xu H, Jia Y, Sun Z, Su J, Liu QS, Zhou Q, *et al.* Environmental Pollution, A Hidden Culprit for Health Issues. *Eco-Environment & Health*. 2022;31-54. doi:10.1016/j.eehl.2022.04.003.
- Inobeme A, Nayak V, Mathew TJ, Okonkwo S, Ekwoba L, Ajai AI, *et al.* Chemometric approach in environmental pollution analysis: A critical review. *J Environ Manage*. 2022;309:114653. doi:10.1016/j.jenvman.2022.114653.
- Machate O, Schmeller DS, Loyau A, Paschke A, Krauss M, Carmona E, *et al.* Complex chemical cocktail, containing insecticides diazinon and permethrin, drives acute toxicity to crustaceans in mountain lakes. *Sci Total Environ*. 2022;828:154456. doi:10.1016/j.scitotenv.2022.154456.
- Lopes T. S. d. A., Hebler R., Bohner, C, Junior, G.B.A., Sena, R. F.D. Pesticides removal from industrial wastewater by a membrane bioreactor and post-treatment with either activated carbon, reverse osmosis or ozonation. *J Environ Chem Eng*. 2020;8(6): p. 104538. doi:10.1016/j.jece. 2020.104538
- Kodali J, Talasila S, Arunraj B, Nagarathnam, R. Activated Coconut Charcoal as a super adsorbent for the removal of organophosphorous pesticide monocrotophos from water. *Case Studies in Chemical and Environmental Engineering*. 2021;3:p.100099. doi:10.1016/j.cscee.2021.100099
- Farghali R, A., Sobhi, M., Gaber, S. E., Ibrahim, H., Elshehy, E. A. Adsorption of organochlorine pesticides on modified porous Al30/bentonite: Kinetic and thermodynamic studies. *Arab J Chem*. 2020;13(8):6730-6740. doi:10.1016/j.arabjc. 2020.06.027.
- Babacan T, Doğan D, Erdem Ü, Metin AÜ. Magnetically responsive chitosan-based nanoparticles for remediation of anionic dyes: Adsorption and magnetically triggered desorption. *Mater Chem Phys*. 2022;284:126032. doi:10.1016/j.matchemphys.2022.126032.
- Pan C. and Liu P, Palygorskite-based self-separable nano-adsorbent for wastewater treatment. *Appl Clay Sci*. 2023;239:p. 106955. doi:10.1016/j.clay.2023.106955
- Toubi F, Deezagi A, Singh G, Oghabian MA, Fatemi SSA, Arpanaei A. Preparation and Characterization of Double Shell Fe<sub>3</sub>O<sub>4</sub> Cluster@Nonporous SiO<sub>2</sub>@Mesoporous SiO<sub>2</sub> Nanocomposite Spheres and Investigation of their *In Vitro* Biocompatibility. *Iran J Biotechnol*. 2015;13(1):1-10.doi:10. 15171/IJB.1068
- Jabbar KQ, Barzinjy AA, Hamad SM. Iron oxide nanoparticles: Preparation methods, functions, adsorption and coagulation/flocculation in wastewater treatment. *Environ Nanotechnol Monit Manag*. 2022;17:100661. doi:10. 1016/j.enmm.2022.100661.
- Rahimi E, Rezaei S, Mohamadnia S, Valizadeh S, Tavakoli O, Faramarzi MA. Bioremoval and Detoxification of Anthracene by a Halophilic Laccase from *Alkalibacillus salilacus*. *Iran J Biotechnol*. 2022;20(2):67-78.doi: 10.30498/IJB.2022.287500.3058.
- Chittal V, Gracias M, Anu A, Saha P, Bhaskara Rao KV. Biodecolorization and Biodegradation of Azo Dye Reactive Orange-16 by Marine *Nocardopsis* sp. *Iran J Biotechnol*. 2019;17(3):18-26.doi: 10.29252/IJB.1551
- Khan A, Malik S, Ali N, Yang Y, Akhter MS, Bilal M. Chapter 2 - Introduction to nano-biosorbents. In: Denizli A, Ali N, Bilal M, Khan A, Nguyen TA, editors. *Nano-Biosorbents for Decontamination of Water, Air, and Soil Pollution: Elsevier*. 2022. p. 29-43.
- Parastar M, Sheshmani S, Shokrollahzadeh S. Cross-linked chitosan into graphene oxide-iron(III) oxide hydroxide as nano-biosorbent for Pd(II) and Cd(II) removal. *Int J Biol Macromol*. 2021;166:229-237. doi: 10.1016/j.ijbiomac.2020.10.160.
- Oktay B, Eroğlu GÖ, Demir S, Kuruca SE, Apohan NK. Poly(lactic acid) nanofibers containing phosphorylcholine grafts for transdermal drug delivery systems. *Mater Today Sustain*. 2022;18:100132. doi:10.1016/j.mtsust.2022.100132.
- Cid-Samamed A, Rakmai J, Mejuto JC, Simal-Gandara J, Astray G. Cyclodextrins inclusion complex: Preparation methods, analytical techniques and food industry applications. *Food Chem*. 2022;384:132467. doi:10.1016/j.foodchem. 2022.132467.
- Mirtajaddini SA, Fathi Najafi M, Vaziri Yazdi SA, Kazemi Oskuee R. Preparation of Chitosan Nanoparticles as a Capable Carrier for Antigen Delivery and Antibody Production. *Iran J Biotechnol*. 2021;19(4):32-40. doi:10.30498/ijb.2021. 247747.2871.

18. Douzandeh-Mobarrez B, Ansari-Dogaheh M, Eslaminejad T, Kazempour M, Shakibaie M. Preparation and Evaluation of the Antibacterial Effect of Magnetic Nanoparticles Containing Gentamicin: A Preliminary In vitro Study. *Iran J Biotechnol.* 2018;**16**(4):287-93. doi:10.21859/ijb.1559.
19. Begum Q, Kalam M, Kamal M, Mahboob T. Biosynthesis, Characterization, and Antibacterial Activity of Silver Nanoparticles Derived from Aloe barbadensis Miller Leaf Extract. *Iran J Biotechnol.* 2020;**18**(2):74-81. doi:10.30498/ijb.2020.145075.2383.
20. Nezamabadi, V., Akhgar, M. R., Tahamipour, B, Rajaei, P. Biosynthesis and Antibacterial Activity of ZnO Nanoparticles by Artemisia Aucheri Extract. *Iran J Biotechnol.* 2020;**18**(2):82-91. doi:10.30498/ijb.2020.151379.2426.
21. Safavinia L, Akhgar MR, Tahamipour B, Ahmadi SA. Green Synthesis of Highly Dispersed Zinc Oxide Nanoparticles Supported on Silica Gel Matrix by Daphne oleoides Extract and their Antibacterial Activity. *Iran J Biotechnol.* 2021;**19**(1):86-95. doi:10.30498/IJB.2021.2598.
22. Yusefi M, Shameli K, Su Yee O, Teow SY, Hedayatnasab Z, Jahangirian H, *et al.* Green Synthesis of Fe<sub>3</sub>O<sub>4</sub> Nanoparticles Stabilized by a Garcinia mangostana Fruit Peel Extract for Hyperthermia and Anticancer Activities. *Int J Nanomed.* 2021;**16**:2515-2532. doi:10.2147/IJN.S284134
23. Yew YP, Shameli K, Miyake M, Kuwano N, Bt Ahmad Khairudin NB, Bt Mohamad SE, *et al.* Green Synthesis of Magnetite (Fe<sub>3</sub>O<sub>4</sub>) Nanoparticles Using Seaweed (Kappaphycus alvarezii) Extract. *Nanoscale Res Lett.* 2016;**11**(1):276. doi:10.1186/s11671-016-1498-2.
24. Kiwumulo HF, Muwonge H, Ibingira C, Lubwama M, Kirabira JB, Ssekitoleko RT. Green synthesis and characterization of iron-oxide nanoparticles using Moringa oleifera: a potential protocol for use in low and middle income countries. *BMC Research Notes.* 2022;**15**(1):149. doi:10.1186/s13104-022-06039-7
25. Mumivand H, Aghemiri A, Aghemiri A, Morshedloo MR, Nikoumanesh K. Ferulago angulata and Tetrataenium lasiopetalum: Essential oils composition and antibacterial activity of the oils and extracts. *Biocatal Agric Biotechnol.* 2019;**22**:101407. doi:10.1016/j.bcab.2019.101407.
26. Naderi N, Hajian M, Souri M, Nasr Esfahani MH, Vash NT. Ferulago angulata extract improves the quality of buck spermatozoa post-thaw and counteracts the harmful effects of diazinon and lead. *Cryobiology.* 2021;**98**:17-24. doi:10.1016/j.cryobiol.2021.01.008.
27. Süzgeç-Selçuk S, Dikpınar T. Phytochemical evaluation of the Ferulago genus and the pharmacological activities of its coumarin constituents. *J Herb Med.* 2021;**25**:100415. doi:10.1016/j.hermed.2020.100415.
28. Yeganeh-Faal, A. and M. Kadkhodaei, A new combustion method for the synthesis of copper oxide nano sheet and Fe<sub>3</sub>O<sub>4</sub>/CuO magnetic nanocomposite and its application in removal of diazinon pesticide. *Results Eng.* 2022;**16**:p.100599. doi:10.1016/j.rineng.2022.100599
29. Shi J, Zhang F, Wu S, Guo Z, Huan X, Hu X, *et al.* Noise-free microbial colony counting method based on hyperspectral features of agar plates. *Food Chem.* 2019;**274**:925-932. doi:10.1016/j.foodchem.2018.09.058
30. Hirad AH, Ansari SA, Ali MAE, Egeh MA. Microwave-mediated synthesis of iron oxide nanoparticles: Photocatalytic, antimicrobial and their cytotoxicity assessment. *Process Biochem.* 2022;**118**:205-214. doi:10.1016/j.procbio.2022.04.022.
31. Yan Z, FitzGerald S, Crawford TM, Mefford OT. Oxidation of wüstite rich iron oxide nanoparticles via post-synthesis annealing. *J Magn Magn Mater.* 2021;**539**:168405. doi:10.1016/j.jmmm.2021.168405
32. Yeste MP, Fernández-Ponce C, Félix E, Tinoco M, Fernández-Cisnal R, García-Villar C, *et al.* Solvothermal synthesis and characterization of ytterbium/iron mixed oxide nanoparticles with potential functionalities for applications as multiplatform contrast agent in medical image techniques. *Ceram Int.* 2022;**48**(21):31191-31202. doi:10.1016/j.ceramint.2022.06.194.
33. Roy SD, Das KC, Dhar SS. Conventional to green synthesis of magnetic iron oxide nanoparticles; its application as catalyst, photocatalyst and toxicity: A short review. *Inorg Chem Commun.* 2021;**134**:109050. doi:10.1016/j.inoche.2021.109050
34. Ghasemi Pirbalouti A, Izadi A, Malek Poor F, Hamed B. Chemical composition, antioxidant and antibacterial activities of essential oils from Ferulago angulata. *Pharm Biol.* 2016;**54**(11):2515-2520. doi:10.3109/13880209.2016.1162816.
35. Tabar Maleki, S. and S.J. Sadati, Synthesis and investigation of hyperthermia properties of Fe<sub>3</sub>O<sub>4</sub>/HNTs magnetic nanocomposite. *Inorg Chem Commun.* 2022;**145**:110000. doi:10.1016/j.inoche.2022.110000
36. Sun C, Li C, Tan H, Zhang Y. Synergistic effects of wood fiber and polylactic acid during co-pyrolysis using TG-FTIR-MS and Py-GC/MS. *Energ Convers Manage.* 2019;**202**:112212. doi:10.1016/j.enconman.2019.112212.
37. Barjasteh-Askari F, *et al.* Photocatalytic removal of diazinon from aqueous solutions: a quantitative systematic review. *Environ Sci Pollut Res.* 2022;**29**(18):26113-26130. doi:10.1007/s11356-022-18743-9
38. Baghersad, M.H., A. Maleki, and M.R. Khodabakhshi, *Design and development of novel magnetic Lentinan/PVA nanocomposite for removal of diazinon, malathion, and diclofenac contaminants. J Contam Hydrol.* 2023;**256**:104193. doi:10.1016/j.jconhyd.2023.104193
39. Abhari, A., *et al.* Thermodynamic Studies on the Adsorption of Organophosphate Pesticides (Diazinon) onto ZnO/Polyethersulfone Nanocomposites. *ChemistrySelect.* 2022;**7**. doi:10.1002/slct.202103619
40. Nikzad S, A.A. Amooey, and A. Alinejad-Mir, High effective removal of diazinon from aqueous solutions using the magnetic tragacanth-montmorillonite nanocomposite: isotherm, kinetic, and mechanism study. *Environ Sci Pollut Res.* 2021;**28**(16):20426-20439. doi:10.1007/s11356-020-12238-1
41. Shamsizadeh, Z., *et al.*, Fe<sub>3</sub>O<sub>4</sub>@SiO<sub>2</sub> magnetic nanocomposites as adsorbents for removal of diazinon from aqueous solution: isotherm and kinetic study. *Pigment Resin Technol.* 2020;**49**:6457-6464. doi:10.1108/PRT-02-2020-0010
42. Heydari S, Zare L, Ghiassi H. Plackett-Burman experimental design for the removal of diazinon pesticide from aqueous system by magnetic bentonite nanocomposites. *J Appl Res Water Wastewater.* 2019;**6**(1):45-50. doi:10.22126/arww.2019.1134
43. Kharat Z, Sadri M, Kabiri M, Herbal Extract Loaded Chitosan/PEO Nanocomposites as Antibacterial Coatings of Orthopaedic Implants. *Fibers Polym.* 2021;**22**(4):989-999. doi:10.1007/s12221-021-0490-3#citeas
44. Dadi R, Azouani R, Traore M, Mielcarek C, Kanaev A. Antibacterial activity of ZnO and CuO nanoparticles against gram positive and gram negative strains. *Mater Sci Eng C Mater Biol Appl.* 2019;**104**:109968. doi:10.1016/j.msec.2019.109968